UDC 621.396.674.3:621.3.029.55
Indexing Terms: Antennas, multiband, Dipole

An HF multiband wire antenna for single-hop point-to-point applications

B. A. AUSTIN, BSc(Eng), MSc(Eng), PhD, FIEE, SenMIEEE, FSAIEE*

SUMMARY

Multiband, as opposed to broadband, antennas can be employed usefully at HF, particularly in tactical and temporary point-to-point applications, if sufficient consideration is given to both ionospheric and geographical conditions. A multiband wire antenna which contains no loading elements nor requires any separate lumped impedance matching networks is analysed and a design methodology is presented. A graphical approach, based on the Smith chart, was used to determine design limits and then a computer-aided procedure optimized the design and developed the various relationships between the antenna elements. Experimental results confirming the validity of the design procedure are included.

* *Department of Electrical Engineering and Electronics, University of Liverpool, PO Box 147, Liverpool L69 3BX; formerly with the Department of Electrical Engineering, University of the Witwatersrand, Johannesburg, South Africa*

1 Introduction

Radio communication circuits at HF (3–30 MHz) are particularly dependent upon the effectiveness of the antenna systems in use at the various terminals. For 24 hour operation over ionospheric paths a number of frequencies must be used in order to operate as close to the prevailing optimum traffic frequency (FOT) as possible. This requirement necessitates that not only must the radio equipment have multi-channel facilities but the antenna systems must likewise be capable of operating effectively on the designated frequencies.

Modern HF transceivers, using frequency synthesis, satisfy the multichannel requirement with relative ease. However, the antenna systems, in general, pose a particular problem, specifically in applications where ease of deployment and possibly tactical requirements demand that only rod, whip or wire antennas may be used. By their nature none of these structures on their own is a wideband device. Hence, some means of matching and possibly resonating the antenna at specified frequencies, or even across bands of frequencies, must be provided. Various methods of achieving this are available[2] and are well known. However, many suffer from particular deficiencies which either limit their usefulness or, worse, seriously degrade their performance. In this paper a wire antenna is described which uses a series-section transmission line transformer to provide better than 2:1 VSWR, at high efficiency, on eight bands of HF frequencies. The particular idea is not new, having originally been popularized by Varney[1] in 1958 for use on the radio amateur frequencies. By using the Smith chart the configuration was analysed and computer software written to optimize its performance. The relationships between the dimensions of the antenna sections were identified, as were those between the bands of frequencies on which it yields the required impedance match. From these, simple design equations were obtained.

2 The Multiband Philosophy

Ideally an HF antenna should provide its required performance in terms of directivity, radiation angle, efficiency and driving point impedance independently of the frequency of operation. Such performance criteria are only possible with a very limited number of antenna structures of which the log-periodic are probably the best known. At HF, though, they are particularly large.

However, only three, suitably selected frequencies would be sufficient for most 24 hour single-hop circuits, thus easing the antenna requirements considerably. Figure 1 shows the predicted[2] optimum traffic frequencies (FOT) for various single-hop paths at 30°S and over a longitude from 0 to 50°E for the month of June 1985. Using the

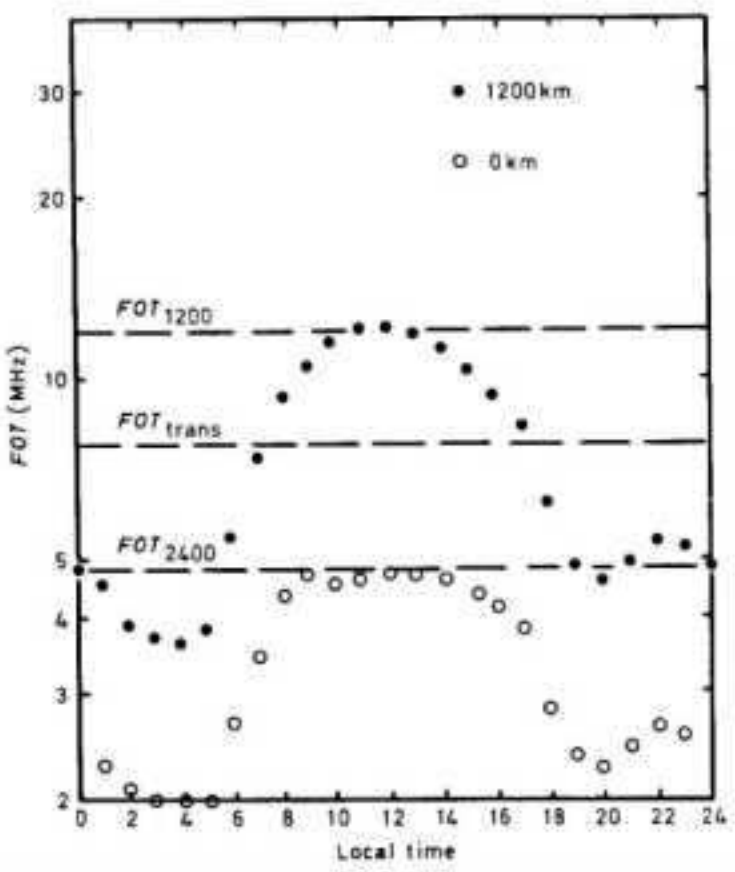

Fig. 1. Optimum traffic frequencies (FOT) for single-hop ionospheric paths at 30°S, 0–50°E, for June 1985.

1200 km data as an example it will be noted that frequencies close to the FOT at noon (FOT_{1200}), midnight (FOT_{2400}) and during the sunrise/sunset transitions (FOT_{trans}) would provide coverage for most of the 24 hour circuit over that path. The ratio FOT_{1200}/FOT_{2400} is the important parameter because it defines the total frequency range required of both transceiver and antenna for the particular communication circuit. For the 1200 km path quoted here, FOT_{1200} is 12·2 MHz while FOT_{2400} is 4·8 MHz. Thus the system frequency range is $12{\cdot}2/4{\cdot}8 = 2{\cdot}54$, which means that the antenna must have the capability of either operating over a bandwidth of somewhat more than an octave; or be adjustable to function near 5 MHz, 12 MHz and on FOT_{trans} of about 8 MHz; or would function automatically on just those three frequencies. This latter option could be provided by the so-called multiband antenna.

For the same circuit in June 1980, when the sunspot number (SSN) was 157, as opposed to the value of 21 in June 1985, the FOT_{1200}/FOT_{2400} ratio was 4·3 with the frequencies to be used being 16·8, 3·9 and a transition frequency of about 9 MHz. It will be noted that not only do the absolute frequencies change over the period of the sunspot cycle, as would be expected, but their ratio changes significantly too, which means that the effective operating bandwidth of the antenna system itself is a variable in the system design equation.

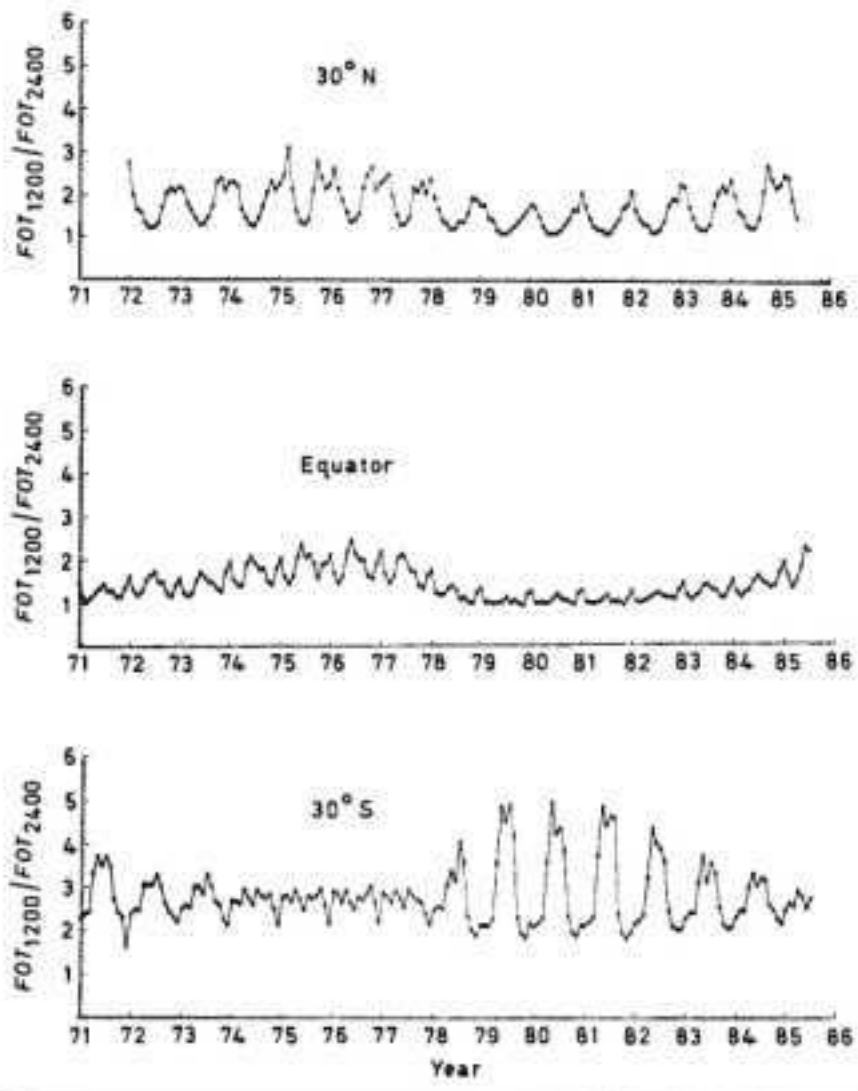

Fig. 2. Variation in FOT_{1200}/FOT_{2400} in three geographical areas for propagation over a 1200 km path.

By way of comparison, 1200 km paths at the equator and at 30°N were analysed and the results, which have been reported elsewhere,[3] are shown, with those of 30°S, in Fig. 2. The differences are marked and exhibit two interesting characteristics: the first being the significant antenna frequency range requirement to be met, particularly during southern hemisphere winter months at low SSN; the second is that the southern hemisphere characteristics are out-of-phase compared with both those at the equator and at 30°N. Finally the antenna requirements are less demanding at the equator and 30°N when the sunspot count is low than when it is high—directly opposite to the 30°S case.

Whereas only the 1200 km, single-hop, path has been discussed here, both 800 km and the so-called zero kilometre (vertical incidence) cases were also examined. Their general characteristics were of the same form as those for the longer path; merely different values of FOT apply.

2.1 Multiband Antenna Options

Multiband performance can be obtained by using the natural harmonic characteristics of halfwave cylindrical antennas to produce a suitable driving-point impedance (and hence impedance match) to low impedance transmission lines on the odd-harmonically related frequencies.[4] Alternatively, a multi-wire structure[5,6] which consists of a number of conductors of dissimilar length, all joined in parallel at the common centre feedpoint, will produce resonances on each of the frequencies at which the individual lengths are approximately a half wavelength. On the other hand a single centre-fed element which contains one or more lumped impedance loading devices, usually parallel LC networks, may be used. These 'traps'[6,7,8] isolate the section between the resonant trap and the end from the feedpoint by virtue of the high impedance which they present to the element at their resonant frequency; at other frequencies they provide reactive loading to the elements. The multiwire and some trap-loaded antennas maintain their directivity at all operating frequencies but the single, unloaded antenna, operating at its natural harmonic frequencies, does not. The electrical length of the antenna changes as the frequency is increased and the radiation pattern becomes multi-lobed.

3 The Single-wire Multiband Antenna with a Series-section Matching Transformer

The geometry of the 'G5RV' antenna is shown in Fig. 3. The antenna element L_1 is connected by the series-section transmission line transformer L_2 of characteristic impedance Z_2 to the transmission line Z_4 and hence to the radio equipment. Clearly L_2 transforms the driving-point impedance, Z_1, of the antenna to Z_3. If Z_3, normalized with respect to Z_4, falls within a defined VSWR circle on the Smith chart then an acceptable match between Z_1 and Z_4 will have been achieved. If L_2 is a low-loss transmission line then the efficiency of the impedance matching process, η_m, is high. This fact, coupled with the naturally high radiation efficiency, η_a, of the unloaded antenna element L_1, if it is not electrically short,[9] implies that the system

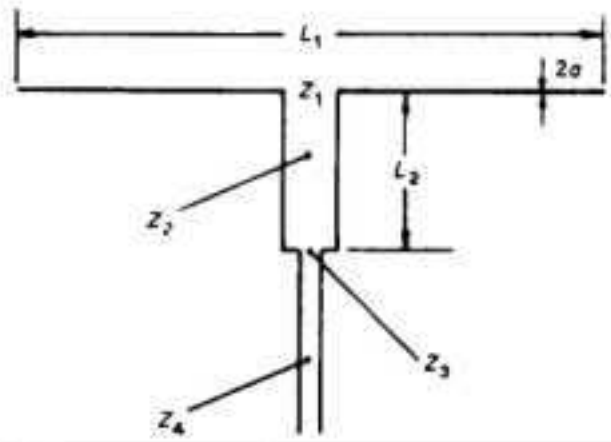

Fig. 3. Geometry of the G5RV multiband antenna.

efficiency $\eta_s = \eta_m \eta_a$ will be high.

L_2 is dependent upon L_1 and their interrelationships, plus that of Z_2, will be illustrated by means of the Smith chart. To enter the chart requires a knowledge of Z_1 and Z_2. Z_1 may be obtained in a number of ways whilst Z_2 is constrained by both practical considerations and by limits which are a function of the impedance matching role played by L_2.

3.1 The Driving-point Impedance of the Antenna

L_1 is a thin-wire element of diameter $2a$ with L_1/a typically 2×10^4. This corresponds to a so-called 'thickness factor' of $\Omega = 2 \ln (L_1/a) \approx 20$. The driving-point impedance, Z_1, could be obtained by solving either Hallen's or Pocklington's integral equations for a thin-wire structure by using techniques such as the Method of Moments.[10] Whereas the technique is both powerful and accurate and a number of computer-based methods exist for its implementation, a procedure which uses published impedance data directly has been followed here.

The standard against which the accuracy of the results obtained from Moment Method techniques is judged has usually been the work of King and his colleagues[11] who have published well-converged results obtained from iterative solutions of Hallen's equations. These constitute the most comprehensive set of driving-point impedance data available and greatly simplify the analytical procedure. These Z_1 data are tabulated in terms of the parameter $k_0 h$ where $k_0 = 2\pi/\lambda$ is the free-space wave number and $h = L_1/2$ is the half-length of the antenna. The parameter is Ω, the conductor thickness factor defined above.

The resistive component, R_1, varies from about 15Ω at $k_0 h = 1$ to more than 4600Ω at $k_0 h = 3{\cdot}0$, while the reactive component X_1 swings from about −2560Ω at $k_0 h = 3{\cdot}1$ to 2146Ω at $k_0 h = 2{\cdot}7$ for the thin-wire antenna denoted by $\Omega = 20$. These impedance data can then be used to develop the impedance matching transformer L_2. For any given value of Z_2 a significant mismatch exists at the junction between L_1 and L_2 on most frequencies. The resulting standing waves cause the intrinsic line losses on L_2 to increase. This effect, which decreases η_m, can be minimized by using low-loss line for L_2. Purely practical considerations limit the range of Z_2 from about 275Ω to 680Ω. With these representative values as the normalization factor and the driving-point impedance, Z_1, provided by the King-Harrison data, the Smith chart can be used to analyse the operation of this multiband antenna.

4 Analysis by Means of the Smith Chart

Z_1 is normalized with respect to Z_2 and the Smith chart entered at the point $Z_{1N} = Z_1/Z_2$ and then transformed by L_2 to $Z_{3N} = Z_3/Z_2$. Z_3 terminates Z_4 and the matching criterion is defined by the VSWR, S, where

$$S = (1 + |\rho|)/(1 - |\rho|) \tag{1}$$

and

$$\rho = (Z_3 - Z_4)/(Z_3 + Z_4) \tag{2}$$

is the reflection coefficient at the junction of L_2 and Z_4.

An acceptable matching criterion is usually $S_{max} = 2:1$. When Z_3 is real the maximum and minimum values of Z_3 which will satisfy the prescribed VSWR condition are

$$Z_{3_{max}} = S_{max} Z_4 \tag{3}$$

and

$$Z_{3_{min}} = Z_4/S_{max} \tag{4}$$

To relate these specific values of Z_3 to Z_1 on the chart, they must be normalized again, this time with respect to Z_2. We thus obtain,

$$Z_{3N_{max}} = (S_{max} Z_4)/Z_2 \tag{5}$$

and

$$Z_{3N_{min}} = Z_4/(S_{max} Z_2) \tag{6}$$

In general the locus of all Z_{3N} values which satisfy the VSWR condition will fall on a circle of diameter d, where

$$d = Z_{3N_{max}} - Z_{3N_{min}} = (Z_4/Z_2)[(S_{max}^2 - 1)/S_{max}] \tag{7}$$

By using a graphical approach like the Smith chart we are effectively identifying certain geometrical conditions which will determine whether an impedance match is possible.

Firstly, Z_{1N} must fall within a defined zone on the chart with limits set by equation (7). The Smith chart in Fig. 4 shows a circle on the real axis, of diameter d, drawn between the limits $(S_{max} Z_4)/Z_2$ and $Z_4/(S_{max} Z_2)$. Any normalized impedance Z_{3N} falling within that circle will then terminate Z_4 such that $VSWR \leqslant S_{max}$. That circle is clearly the target into which Z_1, normalized with respect to Z_2, must fall when rotated by an amount L_2/λ towards the generator (clockwise) around the chart. It is thus referred to in this analysis as the 'target area' (TA).

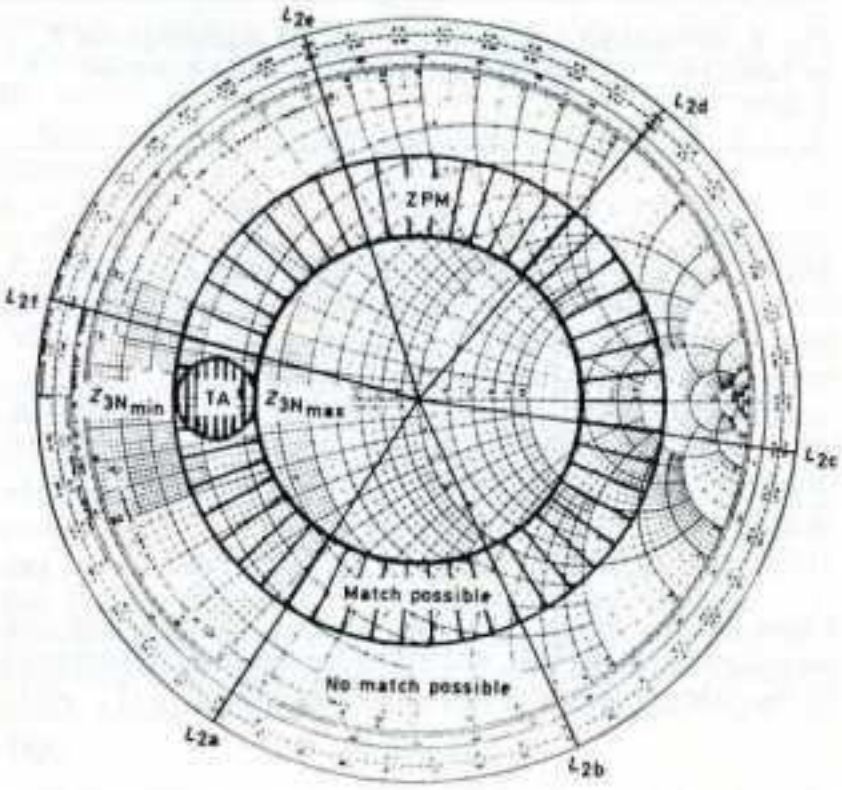

Fig. 4. Smith chart showing the target area and zone of possible matching and the effect of L_2.

Two other geometrical conditions, also shown in Fig. 4, determine matching. The first is the so-called 'zone of possible matching' (ZPM) which falls between two concentric circles centred on the chart and passing through $Z_{3N_{max}}$ and $Z_{3N_{min}}$. The ZPM is thus effectively the locus of the TA around the chart which indicates that only impedances, Z_{1N}, within the ZPM can possibly fall within the TA and so yield a match. This condition thus has implications for the value of Z_2 and these are examined below.

Figure 5 shows the driving-point impedance, Z_1, normalized with respect to three values of Z_2, namely 1000Ω, 350Ω and 100Ω. These are plotted on the Smith chart for $k_0 h$ from 1 to 12, which basically covers the HF spectrum. Each value of Z_2 produces an approximately circular plot of Z_{1N} on the chart. As Z_2 is decreased so the centre of each circle moves to the right. From the matching mechanism discussed above it is clear that optimum matching will occur when the Z_{1N} circle is

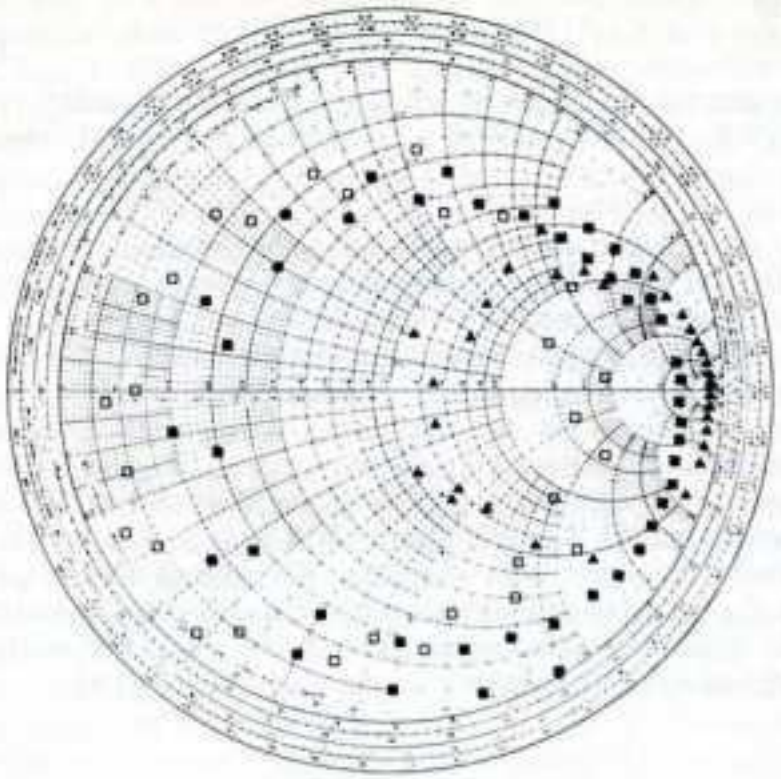

Fig. 5. Normalized antenna driving-point impedance for Z_2 of 1000Ω (□), 350Ω (■) and 100Ω (▲) and k_0h from 1 to 12.

centred on the chart, thus falling within the ZPM. Figure 5 shows this to be best approximated by Z_2 of 350Ω for the three values illustrated. A circular locus will only be maintained around the chart if L_2 is lossless.

L_2 is a fixed physical length. Its action as an impedance transformer is determined by, amongst other things, the fact that its electrical length is a function of frequency. Thus

$$L_{2(\text{elec})} = L_2/\lambda = L_2 f/v \tag{8}$$

where λ is the wavelength and v the velocity of propagation on the line, related to the freespace velocity, c, by the velocity factor, $VF = v/c$. Clearly then

$$L_{2(\text{elec})} = kf \tag{9}$$

where $k = L_2/v$ is a constant.

Only those values of Z_{1N} which coincide on the chart with the particular electrical length of L_{2n} at that frequency, f_n, given by

$$L_{2n} = L_{2a} f_n / f_a \tag{10}$$

where L_{2a} is the equivalent length at frequency f_a, will map into the TA.

This graphical procedure using the Smith chart is a most effective way of illustrating the operating mechanism of this antenna. It does not, however, lend itself easily to design. This can be very readily handled though on a computer and will be described in the next section.

5 Computer-based Analysis and Synthesis

Given the driving-point impedance data for a particular length L_1 and any frequency of interest, Z_3 is obtained from the transmission line equation. If L_2 has minimal loss then, with $\beta = 2\pi/\lambda$,

$$Z_3 = R_3 \pm jX_3 \approx \frac{Z_2(Z_1 + jZ_2 \tan \beta L_2)}{Z_2 + jZ_1 \tan \beta L_2} \tag{11}$$

where

$$R_3 = \frac{R_1(1+\tan^2 \beta L_2)}{[1-(X_1/X_2)\tan \beta L_2]^2 + [(R_1/Z_2)\tan \beta L_2]^2} \tag{12}$$

and

$$X_3 = \frac{X_1(1-\tan^2 \beta L_2) + Z_2[1-(R_1/Z_2)^2-(X_1/Z_2)^2]\tan \beta L_2}{[1-(X_1/X_2)\tan \beta L_2]^2 + [(R_1/Z_2)\tan \beta L_2]^2} \tag{13}$$

Using equations (11)–(13) both analysis and synthesis programs were written with the Z_1 source data in a look-up table.

In the synthesis program L_1, L_2 and Z_2 are changed within reasonable limits while seeking those combinations which produce the required impedance match to Z_4 at the greatest number of frequencies. This search produced the data for Fig. 6, which shows the probability of a particular value of Z_2 yielding such a match for a range of values of L_1 and L_2. It will be noted that the distribution strongly favours Z_2 between about 325Ω and 400Ω, as implied in Fig. 5.

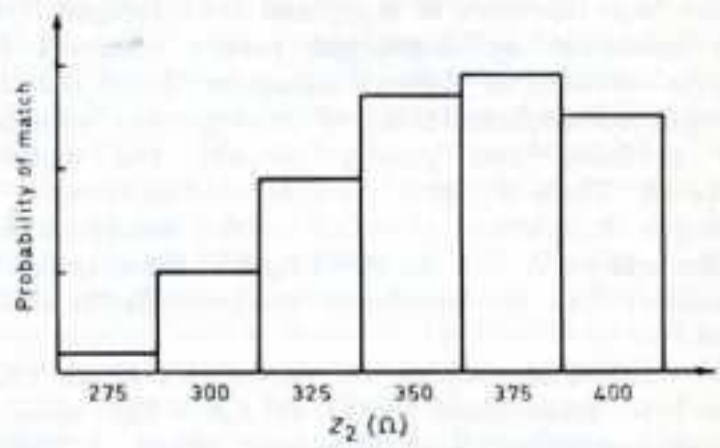

Fig. 6. Probability of particular values of Z_2 yielding the acceptable match.

Likewise those lengths of L_1 and L_2 which produced the required match are shown in terms of $f_{\min}$, the lowest frequency at which a match occurred, in Figs 7(a) and (b) with respect to Z_2 over its optimum range identified above.

Linear regression using the mean values of $L_1 f_{\min}$ and $L_2 f_{\min}$ produced

$$L_1 f_{\min} = 218{\cdot}26 - 0{\cdot}0472 Z_2 \tag{14}$$

and

$$L_2 f_{\min} = 86{\cdot}5 + 0{\cdot}016 Z_2 \tag{15}$$

Now, from Fig. 6 the matching performance of the antenna system is roughly independent of Z_2 between 325Ω and 400Ω; thus, Z_2 can be eliminated from (14) and (15) by solving them simultaneously to yield

$$L_1 f_{\min} = 473{\cdot}44 - 2{\cdot}95\, L_2 f_{\min} \tag{16}$$

These equations and the frequency relationships to be presented in the next section can now be used to design this multiband antenna system.

5.1 The Frequencies of Optimum Match

Table 1 shows how the frequencies at which the lowest VSWR occurs are related for three values of Z_2, namely 275Ω, 350Ω and 400Ω. These frequencies are normalized with respect to $f_{\min}$ in each case and are shown as a series in $f_N = f/f_{\min}$.

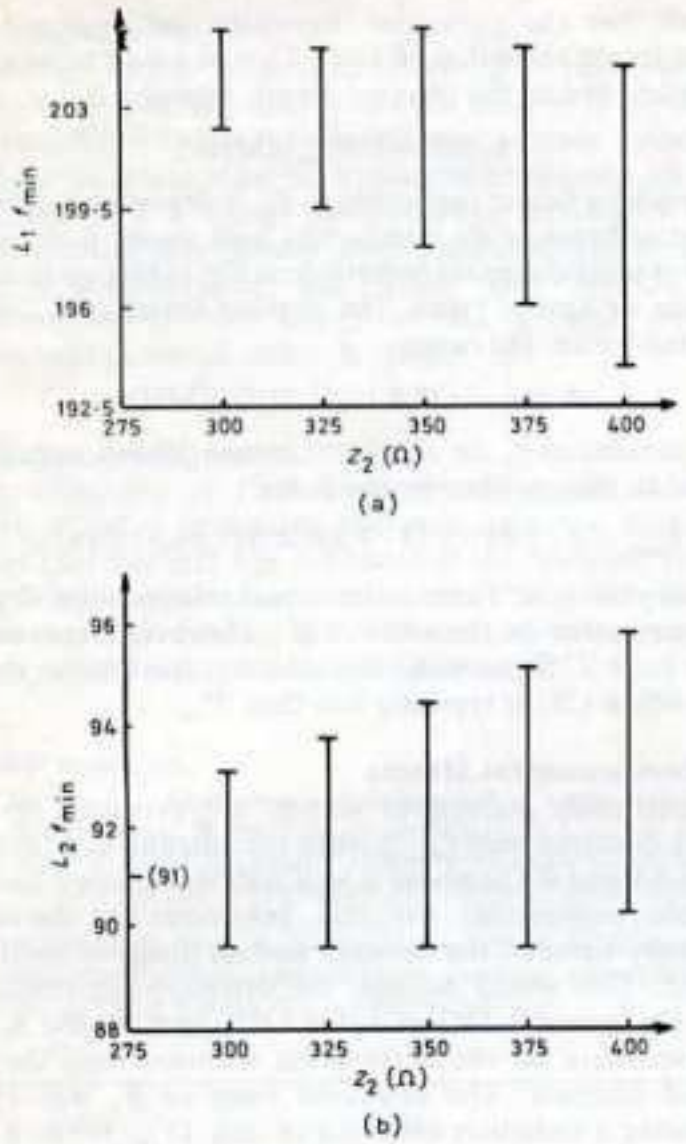

Fig. 7. Ranges of (a) $L_1 f_{min}$ and (b) $L_2 f_{min}$ with Z_2 which produce a match.

For the particular case of $Z_2 = 350\Omega$, Table 2 shows the computed minimum VSWRs for the first fifteen frequencies in the series. Only $N = 2$ and $N = 4$ of the even values of N (N is the first, second, third, etc. frequency at which a match occurs) yield a VSWR better than 2 : 1, whereas all odd values of N in the table do so. Using the Smith chart approach outlined above these fifteen cases are all shown in Fig. 8. The data were obtained by using the synthesis program to obtain L_1 and L_2 for $Z_2 = 350\Omega$ and then $k_0 h$ was calculated at each frequency in the f_N series. The King–Harrison driving-point impedance tabulation yielded Z_1 which was then normalized with respect to Z_2 and plotted on the Smith chart.

The analytical technique using the computer and the graphical approach on the Smith chart are seen to agree thereby confirming the validity and usefulness of each.

Figure 8 and Table 2 show that this multiband antenna will operate on eight bands of frequencies between 3 and 30 MHz. Its effective use, of course, requires that due attention be paid to the ionospheric and geographical factors discussed in Section 2.

Table 1. Computed frequency relationships for optimum matching with three values of Z_2

$Z_2(\Omega)$	f_N
275	1 : 2·07 : 2·60 : 3·60 : 4·21
350	1 : 2·01 : 2·54 : 3·52 : 4·09
400	1 : 1·97 : 2·52 : 3·47 : 4·04

Table 2. Computed relative frequencies at which minimum VSWR occurs for the case $Z_2 = 350\Omega$

N	f_N	$VSWR_{min}$
1	1·0	1·08
2	2·01	1·11
3	2·54	1·09
4	3·52	1·48
5	4·09	1·14
6	5·03	2·03
7	5·65	1·16
8	6·53	2·56
9	7·20	1·16
10	8·04	3·00
11	8·76	1·18
12	9·54	3·33
13	10·32	1·22
14	11·04	3·51
15	11·88	1·22

6 Experimental Results

Antennas designed according to equations (14) and (15) were erected from 1 m to 15 m above various groundplane surfaces, ranging from open fields to steel reinforced concrete buildings. Z_3 was measured and the VSWR on Z_4 was calculated. Figure 9 shows one such set of results and the best-fit predicted curves on the five bands examined.

With $f_{min} = 9$ MHz (chosen quite arbitrarily), then from equation (14) $L_1 = 22{\cdot}7$ m and from equation (15) $L_2 = 10{\cdot}14$ m with $Z_2 = 300\Omega$. The computer-predicted configuration which produced the best-fit with the measured results was $L_1 = 22$ m, $L_2 = 9{\cdot}95$ m and $Z_2 = 360\Omega$.

The difference between the values of L_1 is quite consistent with the need to shorten the physical length of a wire antenna to compensate for the effects of finite conductor thickness and that due to non-zero capacitance at the ends. Similarly, the lengths of L_2 differ, to some extent, because of the velocity factor of the transmission line used. However, the predicted value of Z_2 was 360Ω not the 300Ω which was assumed. The characteristic impedance of the cable used was measured over the frequency range of interest and it was found to be closer to 355Ω, which agreed very well with the value predicted.

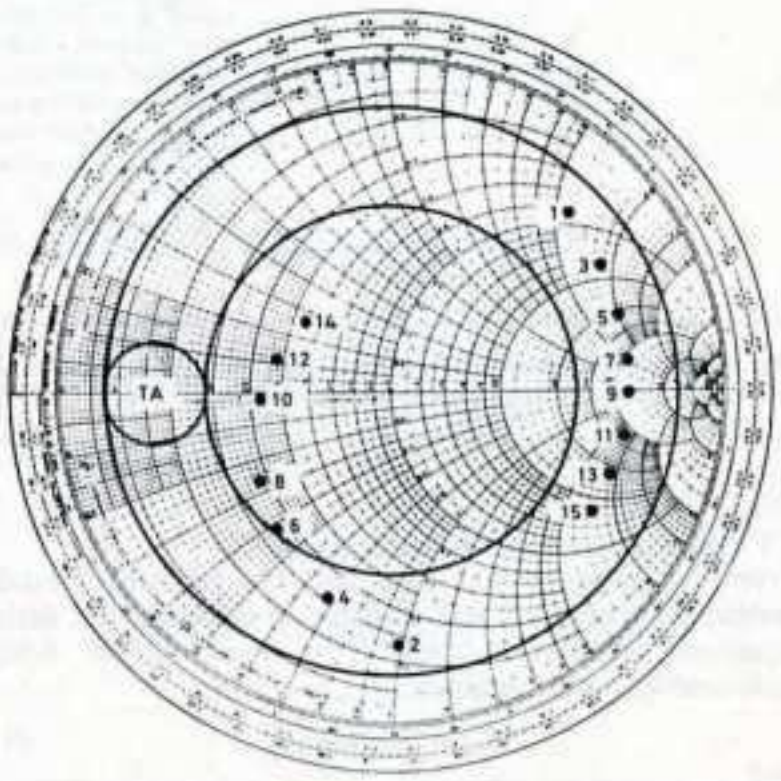

Fig. 8. Driving-point impedances for $N = 1$ to 15 showing possible values which match.

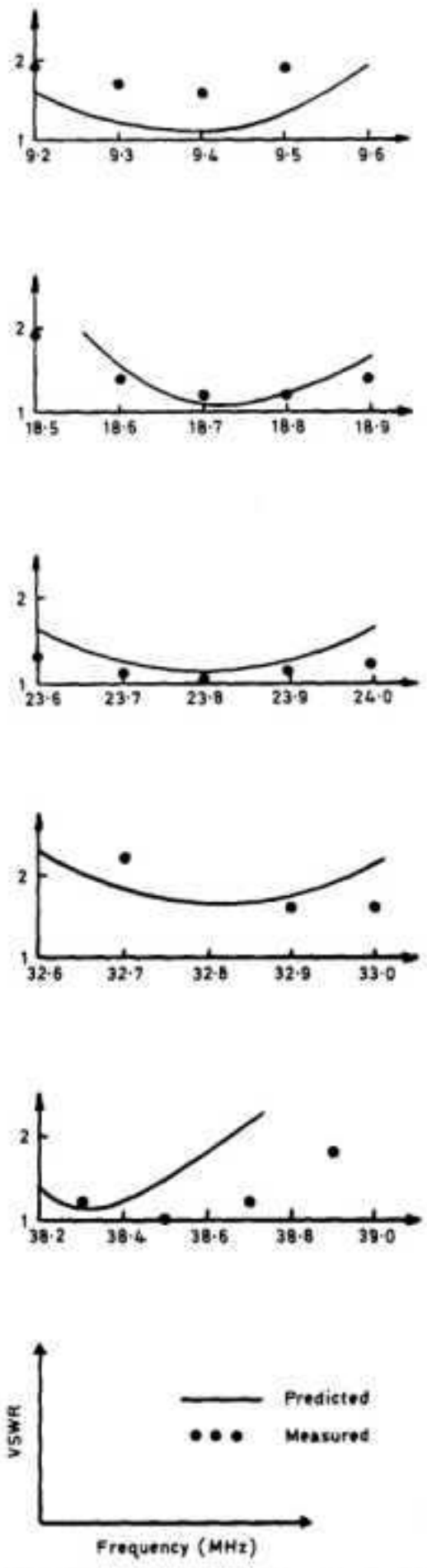

Fig. 9. Measured and best-fit predicted results for the antenna 15 m above ground.

6.1 Optimizing the Design Equations

From the experimental data and the adjusted 'best-fit' system dimensions it was possible to optimize the design equations (14), (15) and (16). Two simple design relationships were obtained:

$$L_1 = 206{\cdot}44/f_{min} \tag{17}$$

and

$$L_2 = 93{\cdot}65/f_{min} \tag{18}$$

where both L_1 and L_2 are electrical dimensions not adjusted for either wire radius, end-effects or velocity factors. For the particular 'thin-wire' installation tested here a length reduction of L_1 of 3% was found to be about optimum; hence, the physical length required is

$$L_1(m) = 200/f_{min}(\text{MHz}) \tag{19}$$

The velocity factor applicable to L_2 is dependent upon the dielectric between its conductors and varies from about 0·80 for solid-dielectric polyethylene flat cables up to about 0·98 for air-spaced types. The physical length of L_2 would then fall within the range

$$L_2(m) = (74{\cdot}9 \text{ to } 91{\cdot}8)/f_{min}(\text{MHz}) \tag{20}$$

The frequencies f_N on which the lowest VSWR occurs are related to one another by the series

$$f/f_{min} = 1 : 1{\cdot}99 : 2{\cdot}53 : 3{\cdot}49 : 4{\cdot}07 : 5{\cdot}62 : 7{\cdot}18 : \ldots \tag{21}$$

As was shown in Table 1 the actual relationships depend to some extent on the value of Z_2. However, between the limits from 275Ω to 400Ω the variation from those shown in equation (21) is typically less than 3%.

6.2 Environmental Effects

An apparently anomalous match, not predicted by the model, occurred near $f_{min}/2$ when the antenna was between about 0·1 and 0·15λ above a well watered, grassed field. A possible explanation for this behaviour is the close proximity between the antenna and its image in the lossy ground. This would increase the driving-point resistance from the nominal 18Ω at $k_0h = 1{\cdot}03$ given by the King–Harrison data for the antenna far removed from the air-ground interface. The measured value of R_1 was 117Ω, suggesting a radiation efficiency of only 15%. While it was not possible to check this, because measurements of radiation efficiency at HF are notoriously difficult,[12] there would appear to be some justification for this assumption in the literature.[13,14] As a horizontal, halfwave antenna approaches to within 0·1λ and closer to the air-ground interface so its resistance increases to a limiting value of about 100Ω. The amount of change is also dependent upon the ground conductivity with the effect being most pronounced with the conductivity in the range from 10^{-2} Sm^{-1} to 10^{-3} Sm^{-1} and high values of permittivity. Using the antenna under test as a geological probe, following Nicol,[15] the ground characteristics were found to be $\sigma = 1{\cdot}14 \times 10^{-2}$ Sm^{-1} and $\varepsilon_r = 28$, which are reasonable and so lend some credence to the actual measured driving-point impedance and to the postulated mechanism at work.

As the excitation frequency was increased, so the ground effects became less marked and the antenna behaved as predicted. Table 3 compares measured values of VSWR at heights from 3 to 13 m above the ground for the first five values of the f_N series plus that of $f/f_{min} = 0{\cdot}5$, the anomalous result. Also shown are the predicted values for the antenna in freespace ($ht = \infty$).

Table 3. The effects of height and frequency on the VSWR for $L_1 = 26{\cdot}5$ m, $L_2 = 12{\cdot}2$ m, $Z_2 = 400\Omega$, $VF = 0{\cdot}897$. (— indicates no data available)

ht (m)	*VSWR* for f_N = 0·5	1	2	2·5	3·5	4·0
3	5·5	1·5	1·5	1·3	1·3	1·7
5	2·8	1·4	1·1	1·6	—	2·0
7	5·0	1·2	1·3	2·0	1·2	—
9	1·9	1·2	1·2	1·6	1·1	—
11	2·5	1·3	1·3	1·5	1·9	1·9
13	1·5	1·6	1·1	1·4	1·1	—
∞	11·8	1·8	1·3	1·6	1·9	1·8

7 Conclusions

By recognizing how the characteristics of the ionosphere vary, both geographically and with time, it is possible to use multiband rather than broadband antenna systems for 24 hour coverage. One such multiband antenna has been analysed and a design methodology developed for it. Experimental results have been presented which validate the procedures used and which also provide some information on the effects of the ground on such horizontal antennas at low heights.

8 Acknowledgments

The assistance of Paul Diepenbroek, Geoff Love and Mark Whalley in making the measurements, that of the Chief Director and Jim Archbold of the National Institute for Telecommunications Research (CSIR) in providing ionospheric predictions and of Glenn Hobbs for processing them, are all very gratefully acknowledged.

9 References

1 Varney, L., 'An effective multiband aerial of simple construction', *RSGB Bulletin*, **34**, no. 7, pp. 19–20, July 1958.

2 NITR (National Institute for Telecommunications Research, CSIR), 'Radio Propagation Predictions for Southern Africa', Series ETP, 1985.

3 Austin, B. A., 'Ionospheric and geographical effects on the choice of tactical and point-to-point HF antenna systems', *Electronics Letters*, **21**, no. 23, pp. 1107–8, 7th November 1985.

4 Radford, M. F., 'High Frequency Antennas', Ch. 16 in 'Handbook of Antenna Design', vol. 2, Rudge, A. W. *et al.* (Eds), pp. 663–724 (Peter Peregrinus, London, 1983).

5 Popovic, B. D., Dragovic, M. B. and Djordjevic, A. R., 'Analysis and Synthesis of Wire Antennas', pp. 105–6 (Research Studies Press, Letchworth, 1982).

6 Grebenkemper, J., 'Multiband trap and parallel HF dipoles—a comparison', *QST*, **64**, no. 5, pp. 26–31, May 1985.

7 Morgan, H. K., 'A multifrequency tuned antenna system', *Electronics*, **13**, pp. 42–8, August 1940.

8 Smith, D. L., 'Trap-loaded cylindrical antenna', *IEEE Trans. on Antennas and Propagation*, **AP-23**, no. 1, pp. 20–7, January 1975.

9 Smith, G. S., 'Efficiency of electrically small antennas combined with matching networks', *IEEE Trans.*, **AP-25**, no. 3, pp. 369–73, May 1977.

10 Moore, J. and Pizer, R., 'Moment Methods in Electromagnetics', pp. 21–66 (Research Studies Press, Letchworth, 1984).

11 King, R. W. P. and Harrison, C. W., 'Antennas and Waves—a Modern Approach', Appx 4, Table A.4.2, pp. 753–7 (The MIT Press, Cambridge, 1969).

12 Smith, G. S., 'An analysis of the Wheeler method for measuring the radiating efficiency of antennas', *IEEE Trans.*, **AP-25**, no. 4, pp. 552–6, July 1977.

13 Rahmat-Samii, Y., Mittra, R. and Parhami, P., 'Evaluation of Sommerfeld integrals for lossy half-space problems', *Electromagnetics*, **1**, no. 1, pp. 1–28, January-March 1981.

14 Burke, G. J., Miller, E. K., Brittingham, J. N., Lager, D. L., Lytle, R. J. and Okada, J. T., 'Computer modelling of antennas near the ground', *Electromagnetics*, **1**, no. 1, pp. 29–49, January-March, 1981.

15 Nicol, J. L., 'The input impedance of horizontal antennas above an imperfect earth', *Radio Science*, **15**, no. 3, pp. 471–7, May-June 1980.

Manuscript first received by the Institution on 6th January 1986 and in revised form on 19th August 1986
Paper No. 2288/COMM433

The Author

B. A. Austin

Brian Austin gained the BSc(Eng) degree in 1969 at the University of the Witwatersrand. He then spent twelve years in industry, mostly with the Research Organization of the Chamber of Mines of South Africa, and led a team that developed a highly rugged, portable SSB transceiver for use in gold mines. His MSc(Eng) degree was awarded in 1976 for a dissertation on MF propagation through lossy stratified media. In 1981 he joined the Department of Electrical Engineering at the University of the Witwatersrand as a Senior Lecturer where his research interests were mainly in HF antennas, numerical modelling and EMC. He was awarded a PhD in 1986 for a thesis on the analysis and evaluation of an HF antenna system operating in a real-world environment. Dr Austin is now with the Department of Electrical Engineering and Electronics at the University of Liverpool.